Ligand-Assisted Inhibition in Cytochrome P450 158A2 from *Streptomyces coelicolor* A3(2)[†,‡]

Bin Zhao,*[,§] Michael R. Waterman,[§] Emre M. Isin,[§] Munirathinam Sundaramoorthy,[§,¶] and Larissa M. Podust[§]

Departments of Biochemistry and Medicine and the Center for Structural Biology, and Center in Molecular Toxicology, Vanderbilt University School of Medicine, Nashville, Tennessee 37232-0146

Received January 30, 2006; Revised Manuscript Received April 27, 2006

ABSTRACT: Cytochrome P450 158A2 (CYP158A2) can polymerize flaviolin to red-brown pigments, which may afford physical protection to the organism, possibly against the deleterious effects of UV radiation. We have found that the small molecule malonic acid enables cocrystallization of this mixed function oxidase with the azole inhibitor 4-phenylimidazole. The presence of malonate molecules affects the behavior of the binding of 4-phenylimidazole to CYP158A2 and increases inhibition potency up to 2-fold compared to 4-phenylimidazole alone. We report here the crystal structure of the 4-phenylimidazole/malonate complex of CYP158A2 at 1.5 Å. Two molecules of malonate used in crystallization are found above the single inhibitor molecule in the active site. Those two molecules are linked between the BC loop and β 1−4/β 6−1 strands via hydrogen bond interactions to stabilize the conformational changes of the BC loop and β strands that take place upon inhibitor binding compared to the ligand-free structure we have reported previously. 4-Phenylimidazole can launch an extensive hydrogen-bonding network in the region of the F/G helices which may stabilize the conformational changes. Our findings clearly show that two molecules of malonate assist the inhibitor 4-phenylimidazole to assume a specific location producing more inhibition in the enzyme catalytic activity.

Cytochromes P450[1] are a superfamily of heme-containing enzymes (more than 5500 known genes, http://drnelson.utmem.edu/CytochromeP450.html) that are involved in a wide array of NADPH-/NADH- and O_2-dependent reactions (*1*, *2*). They have been identified in all biological kingdoms from bacteria to humans (*3*). In eukaryotes, certain P450s have a pivotal role in the biosynthesis of many physiologically important compounds such as steroid hormones and other sterols, vitamins, and eicosanoids (*4*). Others participate in the detoxification of diverse xenobiotic compounds (*5*). P450 inhibition has become a major treatment strategy for P450-mediated diseases. For example, the inhibition of aromatase cytochrome P450 is a primary approach for reducing estrogen-dependent breast cancer (*6*). Inhibition of sterol 14α-demethylase (CYP51) is important for treatment of pathogenic, fungal infections. CYP2A6 inhibition may have potential in treatment of tobacco dependence (*7*).

Streptomyces coelicolor A3(*2*) is the most studied *Streptomyces* species and a model for genetic analysis of production of more than 20 different secondary metabolites, including pigments, antibiotics, siderophores, hopanoids, and other lipids (*8*, *9*). Sequence analysis of the metabolically rich 8.7-Mbp genome of this model actinomycete revealed that there are 18 cytochrome P450 sequences (*10*). Cytochrome P450 158A2 (CYP158A2) is one of these, located in a 3-gene operon which is present in the chromosome of many *Streptomyces* species (*11*, *12*). We have demonstrated that CYP158A2 catalyzes oxidative C−C coupling reactions of the phenol-like molecule flaviolin to biflaviolin and triflaviolin in vitro (*13*). The 3-gene operon is required for biosynthesis of these red-brown pigments through 1,3,6,8-tetrahydroxynaphthalene, which is further oxidized to the CYP158A2 substrate flaviolin (*14*, *15*). These pigments are thought to afford physical protection to this soil bacterium against the deleterious effects of UV radiation (*11*, *16*). To probe the molecular basis of this oxidative C−C coupling reaction, we have determined the CYP158A2 crystal structure with two flaviolin molecules bound in the active site at 1.62 Å (accession code: 1T93) and the substrate-free structure at 1.75 Å (accession code: 1SE6) (*13*). The presence of two flaviolin molecules in the active site implies the reaction of oxidative C−C coupling of these phenolic molecules occurs within the active site. During the early stages of crystallization screening, we found that the enzyme can only be crystallized with the azole inhibitor 4-phenylimidazole in the presence of the additive, malonic acid. Further, we have found that the presence of molecules of malonate can affect the binding of this azole inhibitor to CYP158A2 and also can increase the inhibition potency for catalytic activity. To explore the structural basis of this cooperative inhibition, we

[†] This work was supported by National Institutes of Health Grants GM69970 (M.R.W.), ES00267 (M.R.W.), DK62524 (M.S.), and United States Public Health Service Grant CA90426 (to Professor F. Peter Guengerich).

[‡] The coordinates and structure factor amplitudes have been deposited with the Protein Data Bank, PDB code: 1S1F.

* To whom correspondence should be addressed: Department of Biochemistry, Vanderbilt University School of Medicine, 864 Robinson Research Building, 23rd and Pierce Avenues, Nashville, TN 37232-0146 USA. Tel: 615-343-4644. Fax: 615-343-0704. E-mail: bin.zhao@vanderbilt.edu.

[§] Department of Biochemistry, Vanderbilt University School of Medicine.

[¶] Department of Medicine, Vanderbilt University School of Medicine.

[1] Abbreviations: P450 or CYP, cytochrome P450 monooxygenase; SRS, predicted substrate recognition sequences.

10.1021/bi060193o CCC: $33.50
Published on Web 05/26/2006

Table 1: Data Collection Statistics and MAD Phasing of CYP158A2/4-Phenylimidazole Complex

	Hg derivative			native (heme-iron)		
space group	$P2_12_12_1$			$P2_12_12_1$		
	peak	inflection	remote	peak	inflection	remote
wavelength (Å)	1.0055	1.0089	0.9975	1.72	1.741	1.6513
resolution range (Å)	36−1.5	36−1.5	36−1.5	30−2.1	30−2.1	30−2.1
total observations	398448	366719	383256	167160	159763	166352
unique reflections	55989	54734	60834	52237	51536	47529
completeness %[a]	92.5(85.5)	91.2(86.1)	89.5(82.3)	97.8(93)	96.3(89.9)	95.0(93.8)
$I/\sigma(I)$[a]	27.6(2.5)	23.6(3.2)	20.8(2.7)	12.9(2.8)	12.1(2.5)	11.9(2.1)
R_{merge} %[a]	6.7(49)	6.2(76)	7.2(52)	7.8(37)	8.3(45)	8.1(38)
MAD Phasing[b] Statistics						
resolution range (Å)		20−2.5			20−3.0	
overall *Z*-score		13			8.9	
mean figure of merit		0.35			0.30	
combined overall *Z*-score			76			
combined figure of merit			0.67			

[a] Values in parentheses refer to the highest resolution shell. [b] MAD phasing statistics were calculated with the program SOLVE (*20*).

report the crystal structure of the 4-phenylimidazole/malonate complex of CYP158A2 at 1.5 Å. Interestingly, two molecules of malonate sit in the active site above the inhibitor 4-phenylimidazole, hydrogen bonding with specific secondary structural elements. These two molecules of malonate can occupy similar binding positions to those of the substrates flaviolins. These results are compatible with the capacity of malonate to influence 4-phenylimidazole binding and inhibition behavior to the enzyme. The structure suggests that malonate molecules may assist in reorientation of 4-phenylimidazole in the relatively large active site pocket of this enzyme and serves as a good model to stabilize a single conformation of the inhibitor in the active site, which may contribute to the cooperative effects of drug−drug interactions in P450 inhibition (*17*) and therefore may point to another direction for inhibitor development in P450 research.

EXPERIMENTAL PROCEDURES

Purification, Crystallization, and Data Collection. The CYP158A2 DNA sequence with four C-terminal histidine codons was subcloned into the *Escherichia coli* expression vector pET17b (Novagen, Madison, WI) using the NdeI and HindIII sites, and the recombinant proteins were expressed in the HMS174 (DE3) strain of *E. coli* and purified, as described previously (*13*). Crystals of CYP158A2 were obtained using the hanging-drop vapor diffusion method, in which 2 μL of 16 mg/mL protein solution (10 mM Tris-HCl buffer (pH 7.5), 100 mM NaCl, and 0.5 mM EDTA) containing 3 mM 4-phenylimidazole was mixed with an equal volume of 1.5 M sodium malonate (pH 6.0). At 22 °C, blocklike crystals appeared within days. They grew in three dimensions to an average size of 0.1 mm × 0.1 mm × 0.2 mm. The crystal belongs to the orthorhombic space group $P2_12_12_1$ with the following unit cell parameters: $a = 54.32$ Å, $b = 65.05$ Å, $c = 104.22$ Å. Heavy atom derivatives were prepared by soaking the crystals in a reservoir solution containing 1 mM sodium ethylmercurithiosalicylic acid for 3 h. The cryoprotectant for flash cooling these crystals at liquid nitrogen temperatures was the original reservoir solution supplemented with 15% (v/v) glycerol. The full multiple anomalous dispersion (MAD) data for mercury and iron at three wavelengths (Table 1) were collected at 100 K on the Southeast Regional Collaborative Access Team (SER-CAT) 22-ID beamline at the Advanced Photon Source, Argonne National Laboratory, Argonne, IL. The data were processed and scaled with the HKL package programs HKL2000 (*18*).

Spectral Analysis of Inhibitor Binding. Spectra were recorded using an Aminco DW2a/OLIS spectrophotometer (On-line Instrument Systems, Bogart, GA). The interaction of 4-phenylimidazole with CYP158A2 was examined by perturbation of the heme Soret spectrum. CYP158A2 (1.0 μM) in 20 mM Bis-Tris (2.0 mL, pH 6.0) was divided between two tandem cuvettes. Ethanol was used to dissolve 4-phenylimidazole, and final ethanol concentrations were ≤2% (v/v) during the titrations. The reference cuvette containing an equal concentration of enzyme in buffer was titrated with an equal volume of the vehicle solvent. After thermal equilibration at 23 °C, a baseline was established between 400 and 450 nm. The 4-phenylimidazole−inhibitor complex was generated by adding 4-phenylimidazole (10 mM) to CYP158A2 in 20 mM Bis-Tris (pH 6.0) with or without malonic acid. Sequential additions of this concentrated solution of 4-phenylimidazole gave a final ligand concentration in the range of 20−900 μM, and the difference spectrum was recorded after each titration. The absorbance difference between wavelength maximum and wavelength minimum was plotted against the added ligand concentration. Spectral dissociation constants (K_d) were estimated using GraphPad Prism software (GraphPad Software, Inc., San Diego, CA). For data fitting, a nonlinear regression analysis was applied using the hyperbolic equation: $A = B_{max}[I]/(K_s + [I])$.

Inhibition Studies. Inhibition studies were carried out with flaviolin as substrate in 20 mM Bis-Tris buffer (pH 6.0) containing 10% (v/v) glycerol. The activity assays were determined as described previously (*13*). A 200 μL assay mixture consisted of 0.5 nmol of CYP158A2, 5 nmol flavodoxin, 1 nmol flavodoxin reductase, and 0.13 μmol flaviolin. Inhibitors were added from a 500 mM ethanol stock solution (final ethanol concentration was ≤2% (v/v)) to the reaction mixture containing or not containing 50 mM malonate. Control reactions without inhibitor were performed by adding the same amount of ethanol with or without 50 mM malonate. The half-maximal inhibitor concentration (IC_{50}) was calculated by linear regression analysis of the

degree of inhibition as a function of inhibitor concentration (*19*). The degree of inhibition was expressed as the ratio of the substrate flaviolin consumption rates of uninhibited and inhibited enzyme.

Structure Determination and Refinement. Multiple anomalous dispersion data sets were used to determine the positions of mercury and heme-iron with SOLVE (*20*). Phases were calculated according to these sites also by using SOLVE (*20*) in Table 1, but the anomalous signals were not large enough for complete phase determination. Alternatively, molecular replacement was used with several polyalanine models derived from crystal structures of different cytochrome P450s using the AmoRe molecular replacement program in the CCP4 suite of programs (*21*). It was only successful with CYP165B3/OxyB (accession code: 1LFK), which has 33% sequence identity to CYP158A2. Several sections of the electron density map, especially the core of the structure near the heme, clearly showed the identity of CYP158A2 side chains. However, the molecular replacement phase information was not enough for refinement. The mercury and iron positions located by molecular replacement phase information agreed with their positions calculated from the anomalous difference Patterson maps after appropriate symmetry transformation. The mercury and iron MAD phase sets were combined using SOLVE (*20*), and the resulting phases were improved by solvent flattening using RESOLVE (*20*). The combined phases led to an interpretable electron density map. The initial model was built in O (*22*) using both $|F_o| - |F_c|$ and $2|F_o| - |F_c|$ maps. The 1.5 Å data set collected at 1.0055 Å was used for model refinement using the CNS1.1 (*23*), and 10.2% of the data was set aside for monitoring R_{free}. Several rounds of rigid-body refinement, positional refinement, and simulated annealing were performed at 1.5 Å resolution accompanied with manual rebuilding. There is one molecule in the asymmetric unit cell. The quality of the model was checked using PROCHECK (*24*), and none of the residues were in the disallowed region. The electron density for residues 339 and 340 located in the P450 meander region (*25*) was ambiguous, so these two residues were completely omitted from the final model. The final model contains residues 8−338 and 341−404, a heme group, a 4-phenylimidazole molecule, a glycerol molecule which is on the protein surface, two malonate molecules, two mercury ions (occupancy 0.2) which were included in the refinement, and 328 water molecules. The refinement statistics for the crystal structure are given in Table 2. The coordinates and structure factor amplitudes have been deposited with the Protein Data Bank (accession code: 1S1F). Figures were generated by Setor (*26*) and PyMOL.[2]

Table 2: Data Refinement Statistics of CYP158A2/4-Phenylimidazole Complex

resolution range (Å)	29−1.5
no. of reflections working/test	54123/5513
R_{work}/R_{free} (%)	20.2/21.6
no. non-H atoms	
protein[a]	3053
water molecules	328
heme	43
inhibitor	11
other ligands[b]	14
R_{msd} in bond lengths (Å)	0.006
R_{msd} in bond angles (deg)	1.6
Ramachandran plot	
most favored (%)	93.1
additional allowed (%)	6.0
generously allowed (%)	0.9
disallowed (%)	0.0
mean coordinate error	
Luzatti plot (Å)	0.18
SIGMMAA (Å)	0.12

[a] Residues 8−338 and 341−406. [b] Two malonate molecules.

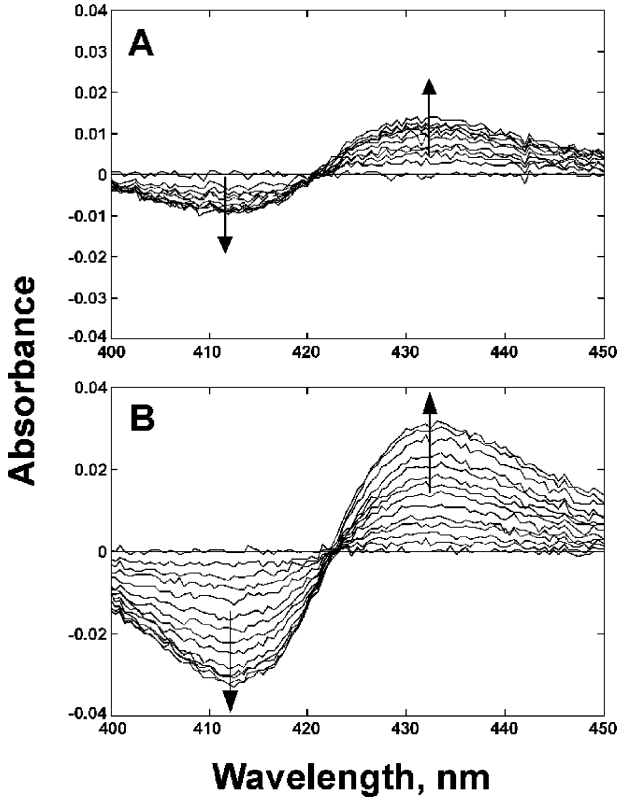

FIGURE 1: Type II binding spectra of CYP158A2 upon addition of increasing concentrations of 4-phenylimidazole (details presented in Experimental Procedures). Spectral changes observed upon titration of CYP158A2 with 4-phenylimidazole (A) in the absence and (B) in the presence of 50 mM sodium malonate.

RESULTS AND DISCUSSION

Inhibitor Binding and Enzyme Inhibition Assay. The experiments in this study were performed at pH 6.0 because the ligand malonic acid has lower pK_a (pK_{a1} 2.85 and pK_{a2} 6.19), and good quality crystals grew at this pH. Spectral titration results show that CYP158A2 binds 4-phenylimidazole, producing a typical type II P450 binding spectrum (Figure 1A), indicating that this azole molecule can coordinate to the heme iron with a rather weak interaction (K_d = 119 ± 7 μM). The binding constant was affected by the presence of malonic acid; the K_d is estimated to be 270 ± 26 μM in the presence of 50 mM malonic acid. It is clear that inhibitor affinity to the enzyme was dependent on the malonic acid concentration, increasing the malonate concentration decreases the binding constant of the inhibitor. Also it is noteworthy that the maximum amplitude of heme spectral change (B_{max}) was increased ~3-fold when malonate was present compared to the P450 alone experiment (Figure 1B). One possible explanation for this would be that 4-phenylimidazole may bind in more than one position in the

[2] DeLano, W. L. (2002) PyMOL Molecular Graphics System at www.pymol.org.

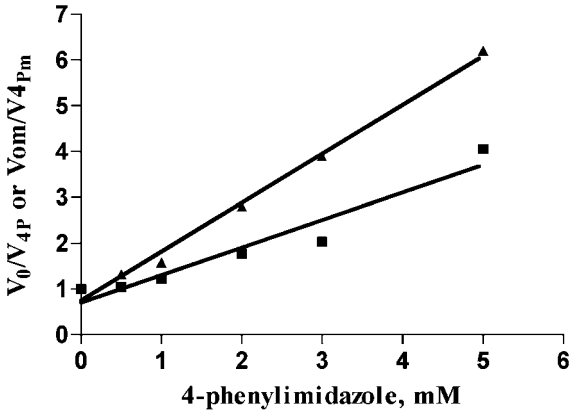

FIGURE 2: Inhibition studies. The rates of flaviolin consumption in the presence and absence of the 50 mM malonate at pH 6.0 were determined as described under Experimental Procedures. The concentration of 4-phenylimidazole is plotted against the ratio of activity measured with or without 50 mM malonate. V_0 and V_{0m} are uninhibited reaction rate with or without malonate, respectively; V_{4P} and V_{4Pm} are inhibited reaction rate using 4-phenylimidazole with or without malonate, respectively. The symbols used are (■) inhibition in the absence of malonate, (▲) inhibition in the presence of malonate.

active site and the presence of malonate causes 4-phenylimidazole reorientation with coordination of the imidzole to the heme iron producing the maximal change in spin state. Alternatively, there may be different populations of the protein in the absence of malonate, some of which may not be able to bind 4-phenylimidazole. Furthermore, to explore whether malonic acid molecules may participate in inhibition of CYP158A2 activity in combination with 4-phenylimidazole, IC_{50} values of 4-phenylimidazole for CYP158A2 were determined at pH 6.0 with or without 50 mM malonate. 4-Phenylimidazole in the presence of 50 mM malonate showed a lower IC_{50} value (1.1 ± 0.2 mM) compared with 4-phenylimidzole alone (2.3 ± 0.1 mM) (Figure 2). This 2-fold increase in the inhibition potency in the presence of the ligand malonate suggests that malonate molecules can help the inhibitor bind into the active site pocket to compete with binding of the substrate flaviolin.

Overall Structure. The CYP158A2 inhibitor−complex structure exhibits the typical P450-fold that consists of α helical and β sheet domains (Figure 3) (*4*, *25*). The overall structure of the inhibitor complex shows a closed conformation in contrast to the open conformation in the ligand-free structure of this enzyme (*13*), but with respect to the flaviolin-bound structure, it is less closed (Figure 4A). The most significant differences between the inhibitor complex and the flaviolin complex are found in the region of the F/G helices (a root-mean-square deviation is 1.1 Å^2 between all F/G region C_α atoms) upon binding of different ligands into the active site (Figure 4A). The F/G helical region is known to be important in substrate binding in other P450s (*4*, *25*, *27*). The BC loop does not show a significant structural difference between these two structures and points into the active site, acting as a "lid" at the entrance of the substrate-binding pocket. The F and G helices are rotated away from the active site about 3° upon inhibitor binding. This apparently results in local distortion of the G helix, which is divided into two halves, an α helix (G) and a 3_{10} helix (G′) accompanied with the rearrangement of other secondary structural elements, similar to the flaviolin-bound complex

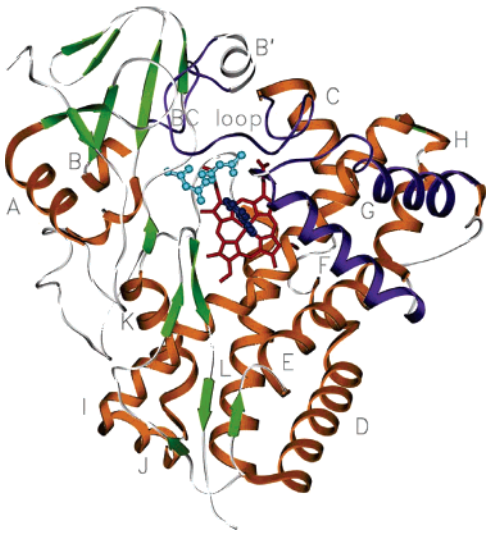

FIGURE 3: A schematic of the overall structure of the CYP158A2 inhibitor complex using a ribbon diagram for the enzyme and a ball-and-stick model for the bound 4-phenylimidazole and two malonate molecules. The α helices are colored orange, β strands green, and random coil white with BC loop and FG region highlighted in purple. The protein ligands of two molecules of malonate and 4-phynelimidazole are colored cyan and indigo, respectively; heme is colored red.

(*13*). The local distortion interrupts the normal hydrogen-bonding pattern of the backbone residues of the G helix so that the N-terminal part of the G helix moves away from the active site and the hydrogen bond interactions between Ile178/Ser188 and Trp174/Glu194 in the F and G helices of the flaviolin complex are broken in the inhibitor complex (Figure 4B,C). Instead, new hydrogen bonds are formed in the kink. A water molecule (WAT500) forms hydrogen bonds with the carbonyl oxygen and carboxyl group of Glu194 of the G helix, which may stabilize the new side chain orientation of Glu194. The amide group of Asn193 forms a hydrogen bond with the amide nitrogen of Glu194. The carboxylate of Glu189 forms a salt bridge with the side chain amide group of Lys192, which provides additional stabilization for this distortion. As a consequence of this local distortion of the G helix, the whole F helix swings away from the structural core. Also the FG loop is positioned out of the active site compared with flaviolin-bound crystal form. The largest movements of F/G loop residues are at Ser188 and Glu189, where the C_α atoms are displaced 5−7 Å. The readjustment of secondary structural elements is required to optimize the hydrogen bonds which stabilize the position of these secondary structural elements. Those conformational changes will explain why the inhibitor complex has a relatively larger active site (665 Å^3) than the substrate flaviolin complex (495 Å^3, calculated using a 1.4 Å probe with the program VOIDOO (*28*)).

The electron density of the two malonate molecules is well-defined in the active site (Figure 5). They exhibit a relatively large substrate-binding pocket of CYP158A2, in agreement with the flaviolin-bound crystal structure (*13*). The average crystallographic temperature factors of proximal and distal malonate molecules are 36.7 and 24.6 Å^2, respectively, indicating distal malonate is relatively more stable than proximal malonate. The distal malonate (M2) is in position to form hydrogen bonds to both the guanidinium group of Arg288 and the amide of Ile87, which acts as a bridge

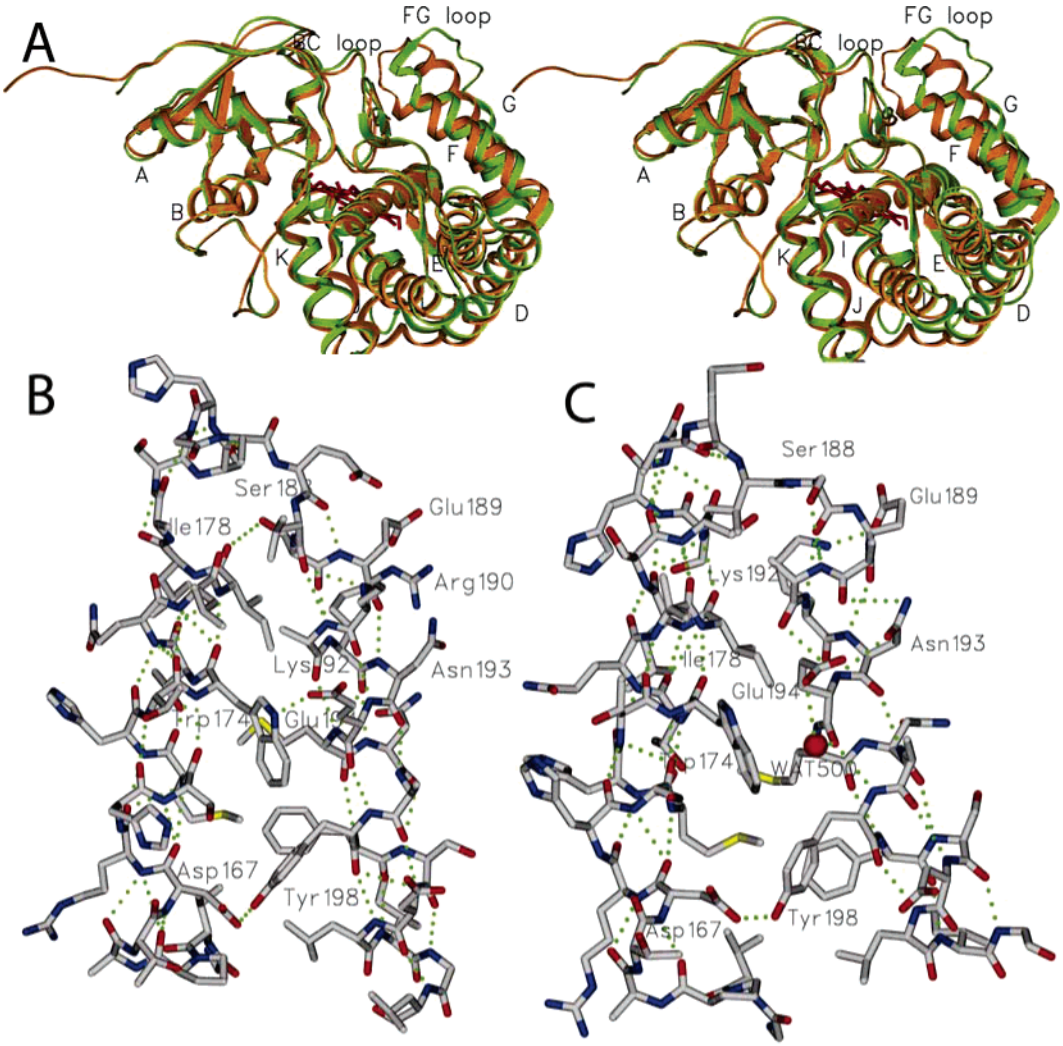

FIGURE 4: (A) Stereoview of the superposition of the 4-phenylimidazole/malonate complex (green) and flaviolin complex structures (orange) with CYP158A2. The heme is colored red. Detailed view of the FG region hydrogen-bonding network formed in flaviolin complex (B) and interrupted hydrogen-bonding pattern in the same region in the inhibitor/malonate complex (C). The hydrogen bond interactions (Ile178/Ser188 and Trp174/Glu194) between F and G helices in the flaviolin complex are lost upon binding of inhibitor and malonate.

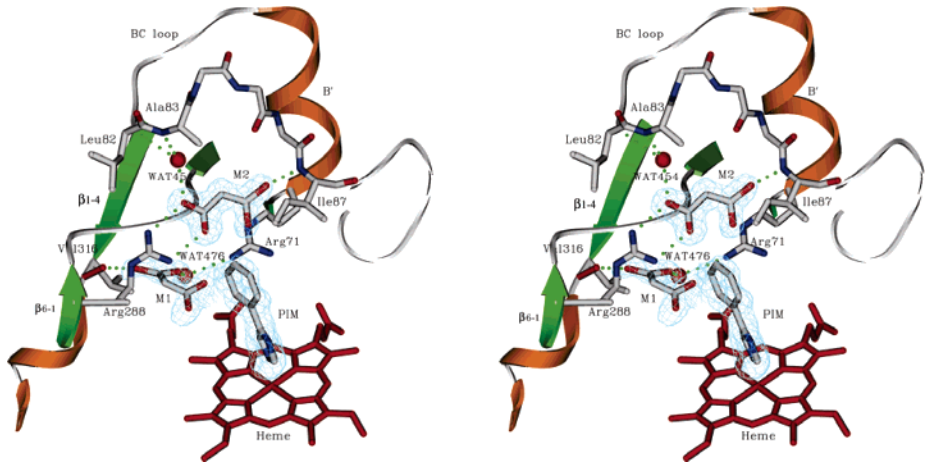

FIGURE 5: Stereoview of the hydrogen-bonding network between residues in the BC loop, ordered waters, and the two malonate molecules in the CYP158A2 active site, $|F_o| - |F_c|$ omit electron density maps of malonates and inhibitor were contoured at 3.0σ. The amino acid atoms Leu82−Ile87 in the BC loop and malonate atoms are rendered as stick figures with the carbons, oxygen, and nitrogen colored gray, red, and blue, respectively. Water molecules are depicted as red spheres. Potential hydrogen bonds are green dotted lines. The proximal and distal malonate molecules in the stick models are denoted "M1" and "M 2", respectively. 4-Phenylimidazole molecule is denoted "PIM".

between the BC loop and strand β 6−1 (Figure 5). It also hydrogen-bonds with the amides of Ala83 and Leu82 via water molecule WAT454. The proximal malonate molecule (M1) only utilizes one side of the carboxyl group to form hydrogen bonds with the carbonyl oxygen of Val316 and interacts with the side chain of Arg71 via water molecule

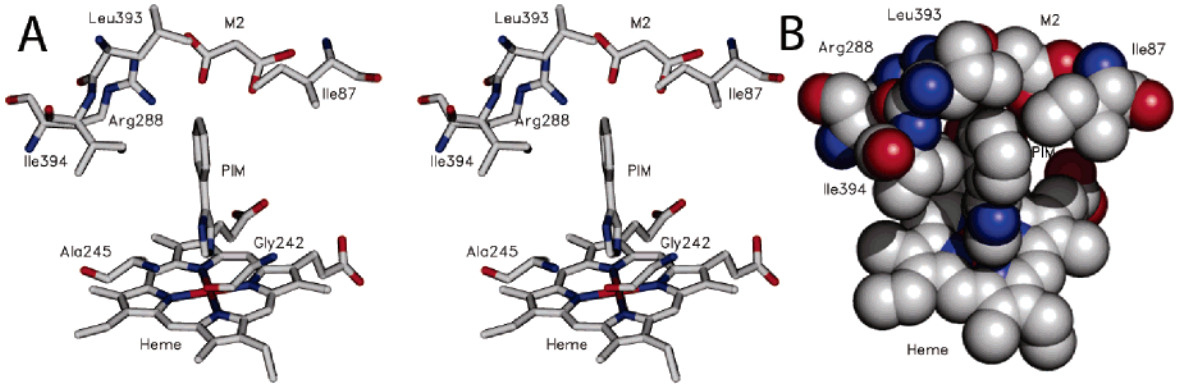

FIGURE 6: (A) The active site residues and distal malonate molecule are rendered as stick figure. Oxygen is shown in red, nitrogen blue, and carbon gray. Stereoview is shown. (B) van der Waals view of hydrophobic cavity created by active site hydrophobic residue side chains of Leu393, Ile394, and Ile87. Note that 4-phenylimidazole fits well into the hydrophobic pocket, and the substrate access channel is blocked by the malonate molecule (M2) and the side chain of Leu393.

WAT476, which is also kinked between the B′ helix and strand β 1−4. The other carboxyl group of the proximal malonate points to 4-phenylimidazole. Hydrogen bond linkages among these secondary structural elements will stabilize the closed conformation of the BC loop region. It is worth noting that the side chains of Arg288 and Arg71 play important roles in CYP158A2 substrate flaviolin binding (*13*). These observations suggest that malonate can compete with flaviolin for the same binding residue side chains. The volume of the inhibitor 4-phenylimidazole is so small compared to the volume of the active site (125 vs 665 Å^3) that it cannot completely stabilize the conformational change without the presence of the two malonate molecules, which is consistent with the results of the inhibitor binding and inhibition behavior being influenced by the malonic acid. These results also can explain why crystals of the enzyme−inhibitor complex do not form in the absence of malonic acid.

Active Site Assay. 4-Phenylimidazole sits in the flaviolin-binding pocket so that the imidazole ring is nearly perpendicular to the porphyrin plane, as one ring nitrogen atom is coordinated to the heme iron (Figure 6A), as observed in 4-phenylimidazole-bound P450$_{cam}$ (*29*). The distance between this nitrogen atom and the heme iron is 2.24 Å, within the normal range (2.13−2.4 Å) of other 4-phenylimidazole-bound P450 structures (*29*−*32*). The 4-phenylimidazole makes several nonbonded contacts with six neighboring residues of the enzyme within 4 Å. These contacting residues are located in the predicted substrate recognition sequences (SRS) (*25*). They are Gly242 and Ala245 in the middle portion of the I helix (SRS-4) coupling with Ile87 from the BC loop (SRS-1), Leu393 and Ile394 from the turn of β-4 (SRS-6), and Arg288 in strand β 6−1 (SRS-5) (Figure 6A). The hydrophobic interactions with 4-phenylimidazole are largely provided by the side chains of Leu393, Ile394, and Ile87 (Figure 6B). They create a relatively large hydrophobic cavity so that the benzene ring of the 4-phenylimidazole can adopt an orientation perpendicular to the axis of the I helix in order to maintain hydrophobic contacts. The side chain of Leu393 is positioned on the top of the phenyl ring, and the side chains of Leu394 and Ile87 lie on both sides of the benzene ring (Figure 6B). The molecule of distal malonate can link the BC loop and β strands to assist in the conformational changes so that the substrate access channel is blocked by the molecule of malonate and the side chain of Leu393, which results in inhibitor 4-phenylimidazole being fixed in the active site once it is bound to the heme iron. This may also explain why either cracking of the crystal or featureless difference Fouriers besides the electron density of 4-phenylimidazole occur when we tried to soak the inhibitor-bound crystal in varying concentrations of flaviolin at different time points, as observed in the crystals of P450BM-3 soaked in a variety of fatty acid substrates yielding featureless difference Fouriers (*33*).

It is interesting to compare ligand binding with enzyme interactions in the active sites of the inhibitor complex and the flaviolin-bound complex. Although the backbone of the protein is changed in the range of 0.5−1.5 Å between these structures, side chains are repositioned differently upon inhibitor binding compared to binding of two molecules of flaviolin (Figure 7). The side chains of Arg71 and Arg288 as well as the amide of Leu293 are directly involved in hydrogen bonding with two substrate molecules of flaviolin in the substrate complex structure (*13*). These hydrogen bonds seem to be important to stabilize and orient substrate in the active site. In the inhibitor complex, the side chains of Arg71 and Arg288 are reoriented slightly resulting from hydrogen bonds with two molecules of malonate. A most obvious difference was that the side chain of Leu293 is rotated 180° in the inhibitor-bound structure (Figure 7), perhaps pointing out that the active site is better designed for flaviolin binding than for binding of 4-phenylimidazole. These perturbations include large, localized changes in the number of water molecules in the active site. There are only two ordered water molecules surrounding the 4-phenylimidazole within 4 Å in the active site pocket, while there are nine ordered water molecules in the flaviolin-bound complex. Those active site water molecules play important roles in proton transfer and dioxygen activation (*34*). On the basis of structural data presented here, it seems that CYP158A2 can adjust both the size (665 Å^3 for inhibitor bound vs 495 Å^3 for flaviolin bound) and polarity of the active site pocket based on the properties of the ligands.

Structural Basis for Conformational Change. There are three other P450 structures with 4-phenylimidazole bound available in the PDB, P450$_{cam}$ (1PHF), CYP119 (1F4T), and CYP51 (1E9X). All show closed conformation compared to their ligand-free structures (*35*, *36*). In CYP158A2, the free imidazole nitrogen atom of 4-phenylimidazole forms an extensive network of hydrogen bonds (Figure 8). An internal

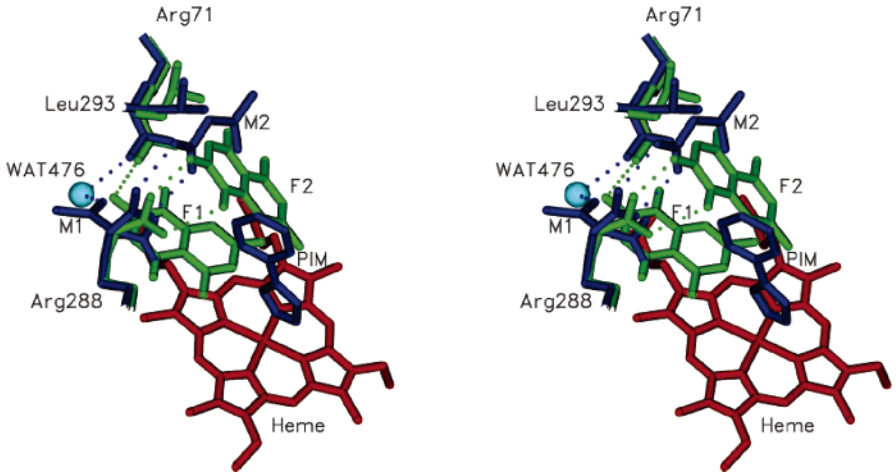

FIGURE 7: Stereoview comparison of the active site of the inhibitor complex (blue) with the active site of the flaviolin complex (green). The bound 4-phenylimidazole is shown in blue; two molecules of malonate are in blue as well; two molecules of flaviolin are in green. The flaviolin molecules are denoted "F1" and "F2".

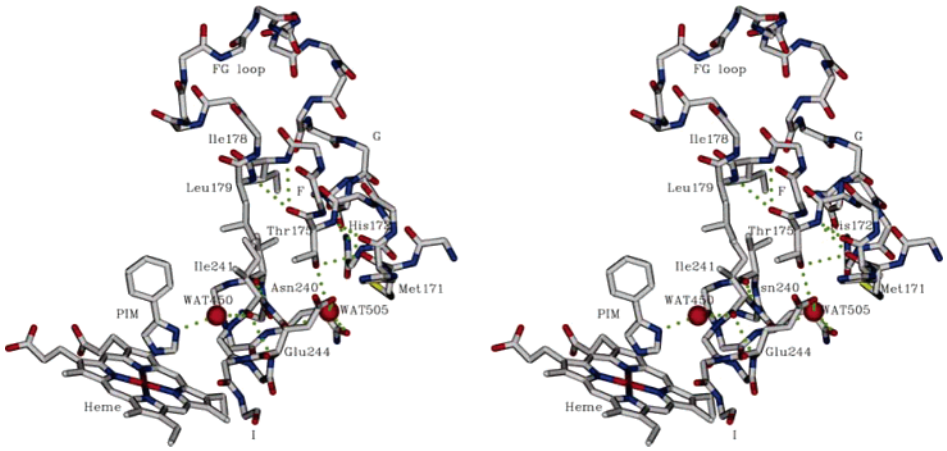

FIGURE 8: Stereoview of the hydrogen-bonding network launched from 4-phenylimidazole which is anchored to Ile241, Glu244, and Asn240 on helix I and makes extensive interaction with the side chain of Thr175 on helix F. The residue atoms, 4-phenylimidazole, and heme atoms are rendered as stick and are colored according to the usual atom types. Water molecules are displayed as red spheres. Potential hydrogen bonds are dotted green lines.

water molecule (WAT450), located nearest to the free nitrogen atom, forms a hydrogen bond with 4-phenylimidazole and also hydrogen-bonds to the backbone carbonyl oxygen of Ile241 that creates the hydrogen-bonding interaction to the backbone amide of Glu244. Both of the side chains of Asn240 and Glu244 are hydrogen-bonded to another internal water molecule (WAT505), which is achieved by hydrogen-bonding interaction with the hydroxyl group of Thr175 on helix F. The crystallographic temperature factors of these two water molecules are 18.3 and 23.4 Å^2, respectively, which indicate they are well-ordered (*29*) owing to taking part in the hydrogen-bonding network with the backbone and side chains of residues in the I and F helices. The inhibitor-induced, hydrogen-bonding pattern coupling with a nonbonded contact as described above is designed to stabilize the conformational change, which is possibly related to the closed/open conformations of the CYP158A2. Hence, the hydrogen-bonding networks via water molecules play an important role in binding 4-phenylimidazole or the polar substrate flaviolin and in stabilizing the significant conformational change in the active site. We also expect that similar hydrogen bond patterns could be present in other P450 complexes with polar substrate bound, as observed in the CYP2C5−diclofenac complex structure (*37*).

In summary, we believe that two molecules of malonate assist in reorientation of the 4-phenylimidazole binding to the relative large volume of the active site and stabilization of the conformational changes for the BC loop and strand β 1−4/β 6−1 via hydrogen bonds. 4-Phenylimidazole can induce a closed conformational change which may help malonate bind to the above secondary structural elements as well. Combining the structural and biochemical results, we find that both the azole inhibitor and ligand malonates are able to compete with flaviolin for the substrate binding site to inhibit activity. As a result, malonate is an important crystallization additive of this stabilization for the 4-phenylimidazole complex of CYP158A2. This study demonstrates how such ligands can fix inhibitor in the active site and consequently increase the inhibition potency for the catalytic activity. These results may help us to understand the cooperative effects of drug−drug interactions in P450 inhibition and may lead to insights into redesigning inhibitor systems for P450s.

ACKNOWLEDGMENT

We thank personnel at SER-CAT 22-ID beamline at APS Argonne National Laboratory for expert technical assistance.

REFERENCES

1. Guengerich, F. P. (1991) Reactions and significance of cytochrome P-450 enzymes, *J. Biol. Chem. 266*, 10019−10022.
2. Porter, T. D., and Coon, M. J. (1991) Cytochrome P-450. Multiplicity of isoforms, substrates, and catalytic and regulatory mechanisms, *J. Biol. Chem. 266*, 13469−13472.
3. Nelson, D. R., Kamataki, T., Waxman, D. J., Guengerich, F. P., Estabrook, R. W., Feyereisen, R., Gonzalez, F. J., Coon, M. J., Gunsalus, I. C., Gotoh, O., and Nebert, D. W. (1993) The P450 superfamily: update on new sequences, gene mapping, accession numbers, early trivial names of enzymes, and nomenclature, *DNA Cell Biol. 12*, 1−51.
4. Ortiz de Montellano, P. R., Ed. (2005) In *Cytochrome P450: Structure, Function and Biochemistry*, pp 323−346, Kluwer Academic/Plenum Publishers, New York.
5. Guengerich, F. P. (2000) Pharmacogenomics of cytochrome P450 and other enzymes involved in biotransformation of xenobiotics, *Drug Dev. Res. 49*, 4−16.
6. Brueggemeier, R. W., Hackett, J. C., and Diaz-Cruz, E. S. (2005) Aromatase inhibitors in the treatment of breast cancer, *Endocr. Rev. 26*, 331−345.
7. Sellers, E. M., Ramamoorthy, Y., Zeman, M. V., Djordjevic, M. V., and Tyndale, R. F. (2003) The effect of methoxsalen on nicotine and 4-(methylnitrosamino)-1-(3-pyridyl)-1-butanone (NNK) metabolism in vivo, *Nicotine Tob. Res. 5*, 891−899.
8. Hopwood, D. A. (1999) Forty years of genetics with *Streptomyces*: from in vivo through in vitro to in silico, *Microbiology 145*, 2183−2203.
9. Bentey, S. D., Chater, K. F., Cerdeno-Tarraga, A. M., Challis, G. L., Thomson, N. R., James, K. D., Harris, D. E., Quail, M. A., Kieser, H., Harper, D., Bateman, A., Brown, S., Chandra, G., Chen, C. W., Collins, M., Cronin, A., Fraser, A., Goble, A., Hidalgo, J., Hornsby, T., Howarth, S., Huang, C. H., Kieser, T., Larke, L., Murphy, L., Oliver, K., O'Neil, S., Rabbiowitsch, E., Rajandream, M. A., Rutherford, K., Rutter, S., Seeger, K., Saunders, D., Sharp, S., Squares, R., Squares, S., Taylor, K., Warren, T., Wietzorrek, A., Woodward, J., Barrell, B. G., Parkhill, J., and Hopwood, D. A. (2002) Complete genome sequence of the model actinomycete *Streptomyces coelicolor* A3(2), *Nature 417*, 141−147.
10. Lamb, D. C., Skaug, T., Song, H.-L., Jackson, C. J., Podust, L. M., Waterman, M. R., Kell, D. B., Kelly, D. E., and Kelly, S. L. (2002) The cytochrome P450 complement (CYPome) of *Streptomyces coelicolor* A3(2), *J. Biol. Chem. 277*, 24000−24005.
11. Cortes, J., Velasco, J., Foster, G., Blackaby, A. P., Rudd, B. A., and Wilkinson, B. (2002) Identification and cloning of a type III polyketide synthase required for diffusible pigment biosynthesis in *Saccharopolyspora erythraea*, *Mol. Microbiol. 44*, 1213−1224.
12. Izumikawa, M., Shipley, P. R., Hopke, J. N., O'Hare, T., Xiang, L., Noel, J. P., and Moore, B. S. (2003) Expression and characterization of the type III polyketide synthase 1,3,6,8-tetrahydroxynaphthalene synthase from *Streptomyces coelicolor* A3(2), *J. Ind. Microbiol. Biotechnol. 30*, 510−515.
13. Zhao, B., Guengerich, F. P., Bellamine, A., Lamb, D. C., Izumikawa, M., Lei, L., Podust, L. M., Sundaramoorthy, M., Reddy, L. M., Kelly, S. L., Kalaitzis, J. A., Stec, D., Voehler, M., Falck, J. R., Moore, B. S., Shimada, T., and Waterman, M. R. (2005) Binding of two flaviolin substrate molecules, oxidative coupling, and crystal structure of *Streptomyces coelicolor* A3(2) cytochrome P450 158A2, *J. Biol. Chem. 280*, 11599−11607.
14. Austin, M. B., Izumikawa, M., Bowman, M. E., Udwary, D. W., Ferrer, J.-L., Moore, B. S., and Noel, J. P. (2004) Crystal structure of a bacterial type III polyketide synthase and enzymatic control of reactive polyketide intermediates, *J. Biol. Chem. 279*, 45162−45174.
15. Funa, N., Funabashi, M., Yoshimura, E., and Horinouchi, S. (2005) A novel quinone-forming monooxygenase family involved in modification of aromatic polyketides, *J. Biol. Chem. 280*, 14514−14523.
16. Funa, N., Funabashi, M., Yoshimura, E., and Horinouchi, S. (2005) Biosynthesis of hexahydroxyperylenequinone melanin via oxidative aryl coupling by cytochrome P-450 in *Streptomyces griseus*, *J. Bacteriol. 187*, 8149−8155.
17. Tang, W., and Stearns, R. A. (2001) Heterotropic cooperativeity of cytochrome P450 3A4 and potential drug-drug interactions, *Curr. Drug Metab. 2*, 185−198.
18. Owtinowski, Z., and Minor, W. (1997) Processing of X-ray diffraction data collected in oscillation mode, in *Macromolecular Crystallography*, Part A, Vol. 276, pp 307−326, Academic Press, New York.
19. Augustinsson, K. B. (1948) Cholinesterases: A study in comparative enzymology, *Acta Physiol. Scand. 15*, 52−60.
20. Terwilliger, T. C., and Berendzen, J. (1999) Automated MAD and MIR structure solution, *Acta Crystallogr., Sect D: Biol. Crystallogr. 55*, 849−861.
21. Collaborative Computational Project, Number 4 (1994) The CCP4 suite: programs for protein crystallography, *Acta Crystallogr., Sect. D: Biol. Crystallogr. 50*, 760−763.
22. Jones, T. A., Zou, J. Y., Cowan, S. W., and Kjeldgaard, M. (1991) Improved methods for building protein models in electron density maps and the location of errors in these models, *Acta Crystallogr., Sect A: Found. Crystallogr. 47*, 110−119.
23. Brunger, A. T., Adams, P. D., Clore, G. M., Delano, W. L., Gros, P., Grosse-Kunstleve, R. W., Jiang, J. S., Kuszewski, J., Nilges, M., and Pannu, N. S. (1998) Crystallography & NMR system: A new software suite for macromolecular structure determination, *Acta Crystallogr., Sect. D: Biol. Crystallogr. 54*, 905−921.
24. Laskowski, R. A., MacArthur, M. W., Moss, D. S., and Thornton, J. M. (1993) PROCHECK: A program to check the stereochemical quality of protein structures, *J. Appl. Crystallogr. 26*, 283−291.
25. Hasemann, C. A., Kurumbail, R. G., Boddupalli, S. S., Peterson, J. A., and Deisenhofer, J. (1995) Structure and function of cytochromes P450: A comparative analysis of three crystal structures, *Structure 15*, 41−62.
26. Evans, S. V. (1993) SETOR: Hardware-lighted three-dimensional solid model representations of macromolecules, *J. Mol. Graphics 11*, 134−138.
27. Gotoh, O. (1992) Substrate recognition sites in cytochrome P450 family 2 (CYP2) proteins inferred from comparative analyses of amino acid and coding nucleotide sequences, *J. Biol. Chem. 267*, 83−90.
28. Kleywegt, G. J., and Jones, T. A. (1994) Detection, delineation, measurement and display of cavities in macromolecular structures, *Acta Crystallogr. Sect. D: Biol. Crystallogr. 50*, 178−185.
29. Poulos, T. L., and Howard, A. J. (1987) Crystal structures of metyrapone- and phenylimidazole-inhibited complexes of cytochrome P-450cam, *Biochemistry 26*, 8165−8174.
30. Yano, J. K., Koo, L. S., Schuller, D. J., Li, H., Ortiz de Montellano, P. R., and Poulos, T. L. (2000) Crystal structure of a thermophilic cytochrome P450 from the archaeon *Sulfolobus solfataricus*, *J. Biol. Chem. 275*, 31086−31092.
31. Podust, L. M., Poulos, T. L., and Waterman, M. R. (2001) Crystal structure of cytochrome P450 14alpha-sterol demethylase (CYP51) from *Mycobacterium tuberculosis* in complex with azole inhibitors, *Proc. Natl. Acad. Sci. U.S.A.* 98, 3068−3073.
32. Podust, L. M., Bach, H., Kim, Y., Lamb, D. C., Arase, M., Kelly, D. H., Sherma, S. L., and Waterman, M. R. (2004) Comparison of the 1.85 Å structure of CYP154A1 from *Streptomyces coelicolor* A3(2) with the closely related CYP154C1 and CYPs from antibiotic biosynthetic pathways, *Protein Sci. 13*, 255−268.
33. Li, H., Poulos, T. L. (1995) Modeling protein-substrate interactions in the heme domain of cytochrome P450(BM-3), *Acta Crystallogr., Sect. D: Biol. Crystallogr. 51*, 21−32.
34. Zhao, B., Guengerich, F. P., Voehler, M., and Waterman, M. R. (2005) Role of active site water molecules and substrate hydroxyl groups in oxygen activation by cytochrome P450 158A2: A new mechanism of proton transfer, *J. Biol. Chem. 280*, 42188−42197.
35. Ravichandran, K. G., Boddupalli, S. S., Hasermann, C. A., Peterson, J. A., and Deisenhofer, J. (1993) Crystal structure of hemoprotein domain of P450BM-3, a prototype for microsomal P450's, *Science 261*, 731−736.
36. Scott, E. E., He, Y. A., Wester, M. R., White, M. A., Chin, C. C., Halpert, J. R., Johnson, E. F., and Stout, C. D. (2003) An open conformation of mammalian cytochrome P450 2B4 at 1.6-Å resolution, *Proc. Natl. Acad. Sci. U.S.A.* 100, 13121−13122.
37. Wester, M. R., Johnson, E. F., Marques-Soares, C., Dijols, S., Dansette, P. M., Mansuy, D., and Stout, C. D. (2003) Structure of mammalian cytochrome P450 2C5 complexed with diclofenac at 2.1 Å resolution: Evidence for an induced fit model of substrate binding, *Biochemistry 42*, 9335−9345.

BI060193O